Bridging the Performance Gap between Electric Double Layer Capacitors and Batteries with High-Energy/High-Power Carbon Nanotube-based Electrodes

*Helena Matabosch Coromina, Beatrice Adeniran, Robert Mokaya, Darren A. Walsh**

School of Chemistry, The University of Nottingham, Nottingham NG7 2RD, UK

E-mail: darren.walsh@nottingham.ac.uk

Keywords: carbon nanotubes; EDLCs; mesoporous materials; energy storage

Abstract

Electric double-layer capacitors (EDLCs) store electrical energy at the interface between charged electrodes and electrolytes and are higher-power devices than batteries. However, the amount of energy stored in EDLCs cannot compete with that in batteries. In this contribution, we describe the development of new EDLCs that can store about as much energy as lead-acid and nickel metal hydride (NiMH) batteries but operate at much higher power densities than achievable using batteries. The electrode materials are derived from carbon nanotubes (CNTs) synthesised from CCl_4 and ferrocene at 180 °C, which is drastically lower than the temperatures usually used to synthesise CNTs. By chemically activating the CNTs using KOH, Bruneuer-Emmett-Teller (BET) surface areas reach ~3000 $m^2\ g^{-1}$, which is orders of magnitude higher than those typical of CNTs, and exceeds even that of pristine graphene. Gas sorption analysis shows that the samples activated at 900 °C contain a mix of micropores and small mesopores, while the samples activated at lower temperatures are predominantly microporous. In EDLCs containing aqueous H_2SO_4 as the electrolyte, the mesoporous carbons exhibit mass-specific capacitances up to 172 F g^{-1}, while in the presence of the ionic liquids 1-ethyl-3-methylimidazolium tetrafluoroborate, [EMIM][BF_4], and 1-butyl-3-methylimidazolium tetrafluoroborate, [BMIM][BF_4], capacitances up to 150 F g^{-1} are measured. Due to the wide potential window of the ionic liquid electrolytes and the unique morphology of the electrode materials, 3-V devices with volume-specific energy densities of the order of 6 Wh L^{-1} and mass specific energy densities up to about 15 Wh kg^{-1} can be fabricated. The energy stored can be delivered at power densities >1 kW kg^{-1} meaning that the performance of these devices bridges the performance gap between those of EDLCs and batteries. The use of this novel electrode material not only allows the fabrication of high-energy/high-power energy storage systems, the methods used to fabricate the electrode materials are inexpensive and can readily be scaled to industrial levels.

1. Introduction

The development of methods for storing electrical energy from alternative but intermittent power sources such as wind turbines and solar panels is an increasingly-important challenge and two of the most promising electrochemical solutions are batteries and EDLCs (sometimes called ultracapacitors or supercapacitors).[1,2] Unlike batteries, in which charge is stored through faradaic charge-transfer reactions, energy is generally stored in EDLCs through simple electrostatic accumulation of charge at the interface between carbon electrodes and liquid electrolytes so these devices can operate at higher charge/discharge rates than batteries (*i.e.*, at higher powers). As no significant structural or chemical changes of the electrode materials occurs during charging/discharging, EDLCs also exhibit significantly longer lifetimes than batteries.[3,4] However, because they only store charge at the electrode/electrolyte interface, the specific energies, E_s, of EDLCs are generally significantly lower (~4–5 Wh kg^{-1}) than those of batteries (~20-400 Wh kg^{-1}) and increasing the energies of EDLCs is a important goal with major societal consequences.[5,6]

In EDLCs, $E_s = \frac{1}{2}CV^2$, where C is the device capacitance and V is the voltage, so increasing E_s involves increasing V and/or the specific capacitance of the electrode materials, C_s. V can be increased by judicious choice of electrolyte; while cells containing aqueous electrolytes are limited to <1.2 V due to the decomposition of water at higher voltages, some organic and ionic-liquid (salts that are liquid below 100 °C) electrolytes can have electrochemical windows up to 3 V and 5 V wide, respectively.[7,8] C_s can be increased by introducing heteroatoms such as oxygen,[9,10] nitrogen,[11,12] or sulfur[13,14] into the carbon structure, or by forming composites with materials such as $Ni(OH)_2$,[15,16] MnO_2,[17,18] polyaniline,[19,20] and polypyrrole.[21-23] Introduction of such pseudocapacitive components, which store charge through faradaic processes, into EDLC electrodes can increase C_s drastically but often at the expense of increased cost and decreased device lifetimes. Perhaps the most common

strategies for increasing C_s in EDLCs are to develop carbon electrode materials with very high specific surface areas (SSAs), and activated carbons (ACs) and graphenes have proven particularly popular.[24-30] However, while ACs can have SSAs in the range 1000–2000 $m^2\ g^{-1}$, they have limited capacitances (~100-200 F g^{-1} in aqueous media and ~50-150 F g^{-1} in organic media[30]) due to a lack of the mesopores necessary for access of charge-balancing counterions to the carbon surface.[31] Graphene has a theoretical SSA of 2680 $m^2\ g^{-1}$ giving a theoretical C_s of 550 F g^{-1} but, in practice, restacking of the graphene sheets during EDLC operation reduces this value significantly.[32] Even after chemical activation of graphene using KOH (which proceeds according to $6KOH + C \rightarrow 2K + 3H_2 + 2K_2CO_3$), which can increase SSA to ~3100 $m^2\ g^{-1}$, the resulting C_s (~160 F g^{-1})[33] is typical of that of ACs in aqueous media.

In contrast to ACs and graphenes, CNTs have not been very widely used as electrode materials for EDLCs to due to their much lower SSAs.[34-37] Some authors have attempted to increase the SSAs of CNTs using KOH activation but the results have not been particularly promising (in terms of the achievable SSAs). Using KOH activation, Kim *et al*. increased the SSA of CNTs from ~400 $m^2\ g^{-1}$ to 650 $m^2\ g^{-1}$,[38] Xu *et al*. achieved an increase from 166 $m^2\ g^{-1}$ to 595 $m^2\ g^{-1}$,[39] and Jiang *et al*. increased SSA from 194 $m^2\ g^{-1}$ to 511 $m^2\ g^{-1}$.[40] A relatively large increase was achieved by Liu *et al*., who increased the SSA of CNTs from 20-30 $m^2\ g^{-1}$ to ~360 $m^2\ g^{-1}$ using relatively large amounts of KOH.[41] Perhaps unsurprisingly, the relatively low SSAs of the such activated materials have resulted in quite modest C_s values when the materials were used as EDLC electrodes; that of Jiang's materials increased from 25 F g^{-1} to 50 F g^{-1},[40] while Xu's measured C_s values increased from ~20 F g^{-1} to ~55 F g^{-1}.[39] Consequently, CNTs have generally not been used as the capacitive component of EDLC electrodes, but have typically been used as additives in EDLC electrodes to increase the power of AC electrodes,[42] or to prevent restacking of graphene sheets.[43]

While the typical C_s of activated CNTs means that they cannot compete with state-of-the-art ACs in EDLCs, the use of CNTs as electrode materials remains an attractive prospect. Due to the high structural rigidity of the CNTs, such electrodes would likely be durable, while mesoporosity (pores in the range 2-50 nm) in CNT-based electrodes could potentially allow facile access of ions to the carbon surface for high-rate charge/discharge operation. However, such a prospect would only be realised if the SSA of CNTs were increased to values as high as those of ACs and graphene, and if a high degree of mesoporosity were introduced during activation. As demonstrated for high-SSA ACs, the development of a high proportion of micropores in the carbons during activation would ultimately limit C_s due to inaccessibility of a large fraction of the electrode surface to ions.[31]

It is known that the degree of graphitisation of CNTs plays a key role during activation of the carbons and the highest increases in SSAs are achieved by chemically activating CNTs with a low degree of graphitisation (i.e. those synthesised at low temperatures).[44] Therefore, it should seem reasonable that CNTs synthesised at very low temperatures could, when activated, potentially make a promising new material for EDLC electrodes. In this contribution we describe the use of CNTs that are synthesised at just 180 °C (which is at least 400 °C lower than conventionally used[44,45]) as the starting material for the synthesis of a high-performance carbon electrode material for 3-V EDLCs. By activating the CNTs with KOH at a range of temperatures, we can tune the surface area and porosity of the resulting materials and, depending on the activation conditions, the BET surface area of the carbons can reach almost 3000 $m^2 g^{-1}$, which exceeds even that of pristine graphene. Crucially, a high degree of mesoporosity can also be retained in the high-SSA carbons during activation and the specific capacitance of the material best-performing material reaches about 170 F g^{-1} in aqueous media. To fabricate a high-energy-density material, we have also combined the material with ionic liquid electrolytes, and devices

containing the ionic liquids [EMIM][BF_4] and [BMIM][BF_4] can operate over a 3-V range. Based on the mass of a fully packaged, [BMIM][BF_4]-containing device, we have achieved mass specific energy densities of the order of 15 Wh kg^{-1} at power densities >1 kW kg^{-1}. Therefore, the use of this new carbon electrode material allows us to bridge a performance gap in the Ragone plot relating the energy and power densities of batteries and EDLCs.

2. Experimental Section

2.1 Materials and Apparatus. General chemicals were obtained from Sigma-Aldrich or Alfa Aesar. [EMIM][BF_4] and [BMIM][BF_4] were synthesised using the methods described in References 46 and 47. Electrochemical measurements were performed using a model 760C potentiostat (CH Instruments, Austin, TX, USA). Powder X-ray diffraction (XRD) analysis was performed using a Bruker D8 Advance powder diffractometer using Cu K_α radiation (λ = 1.5406 Å) and operating at 40 kV and 40 mA. Thermogravimetric analysis (TGA) was performed using a TA Instruments SDT Q600 analyzer from room temperature to 1000 °C at 10 °C min^{-1} in air. Nitrogen sorption isotherms were determined at –196 °C using a Micromeritics ASAP 2020 sorptometer. Scanning electron microscopy (SEM) images were recorded using an FEI XL30 microscope and transmission electron microscopy (TEM) images were obtained using a JOEL 2000-FX electron microscope operating at 200 kV.

2.2 Synthesis of Carbon Nanotubes. In a typical synthesis, ferrocene (3.0 g) was dissolved in CCl_4 (100 mL) to give a yellow mixture, which was stirred at room temperature until completely homogenous. Nickel (10 g) was then added to the mixture, which was heated in an autoclave at 180 °C for 6 hr. The product was then recovered by filtration and washed sequentially with ethanol, 2.0 M HCl and water, and then dried in air to give about 14

g of carbon. To remove non-carbonaceous matter, the product was washed in 15.8 M HNO_3 for 24 h and the resulting material was recovered by filtration and then washed sequentially with ethanol and water.

Activation of the acid-washed materials was performed at KOH/CNT mass ratios of 2:1. The required amount of KOH was crushed to a powder and thoroughly mixed with each CNT sample. The mixtures were placed in a tube furnace and heated at a ramp rate of 3 °C min^{-1} to temperatures between 600 and 900 °C and held at this temperature for 1 hr. The activated materials were then stirred in 2.0 M HCl at room temperature until all inorganic impurities were removed (as confirmed by TGA). The carbons were then filtered, washed with deionised water, and dried at 100 °C for 6 hr. The materials were designated as CN2T, where 2 is the KOH/CNT ratio and T is the activation temperature (°C).

2.3 Materials Characterisation. Surface areas of carbons were determined using the BET method based on adsorption data in the relative pressure (P/P_o) range 0.02-0.22. Prior to analysis, the samples were evacuated for 12 hr at 200 °C under vacuum and the total pore volume was calculated from the amount of nitrogen adsorbed at P/P_o = 0.99. Micropore volumes and surface areas were obtained from t-plot analyses and pore size distributions were obtained from non-local density functional theory (NLDFT) using nitrogen-sorption data. SEM data were recorded by mounting samples on a conductive carbon tape and sputter-coating with a thin (ca. 10 nm) film of Au–Pd to reduce the effects of sample charging. TEM images were obtained by suspending small amounts of the samples in ethanol, which was then deposited and dried on a holey carbon film on a copper grid.

2.4 Electrochemical Measurements. Prior to use, two glassy-carbon plates were polished with an aqueous suspension of 0.3 μm alumina (Buehler, Lake Bluff, Illinois) on felt

polishing pads, sonicated in an ultrasonic bath, and rinsed with deionized water. The CNT samples were mixed with deionised water and 5 wt.% polytetrafluoroethylene (PTFE) binder under sonication for 30 min, giving a uniform suspension. 9 μL of the suspension was then cast onto a glassy carbon plate current collector (14 mm × 10 mm × 2 mm) giving 0.3 mg carbon on each plate. After drying at room temperature, a uniform film was formed on each plate. Sandwich cells were then constructed using the carbon-coated plates, a nanoporous membrane soaked in 2.0 M KCl, 6.0 M KOH, 2.0 M H_2SO_4, [EMIM][BF_4], or [BMIM][BF_4]. Each electrolyte was bubbled with N_2 for 30 min before soaking into the separator and assembled EDLCs were sealed using laboratory film.

3. Results and Discussion

The SEM and TEM images in Figures S1 and S2 in the Supporting Information show that the as-synthesised CNTs have closed tips, diameters ranging from 80 nm at their tips to 300 nm at their base, and form tangled closely-packed networks with few stand-alone or isolated CNTs. The CNTs are also hollow with non-graphitic, ~25 nm-thick walls. After washing with HNO_3, ethanol and H_2O to remove any inorganic residues, the CNTs remain aggregated but have more open tips (Figure S3 and S4 in the Supporting Information). Upon activation with KOH, the walls of the CNTs become porous, while the tubular morphology is retained (Figure 1A-C and Figure S5 and S6 in the Supporting Information). However, the extent to which the tubular morphology is retained decreases at higher activation temperatures (Figure S5 and S6), due to an increase in the level of activation and greater disruption of the original morphology. TGA of the washed carbon confirmed that it is entirely carbonaceous with no residual

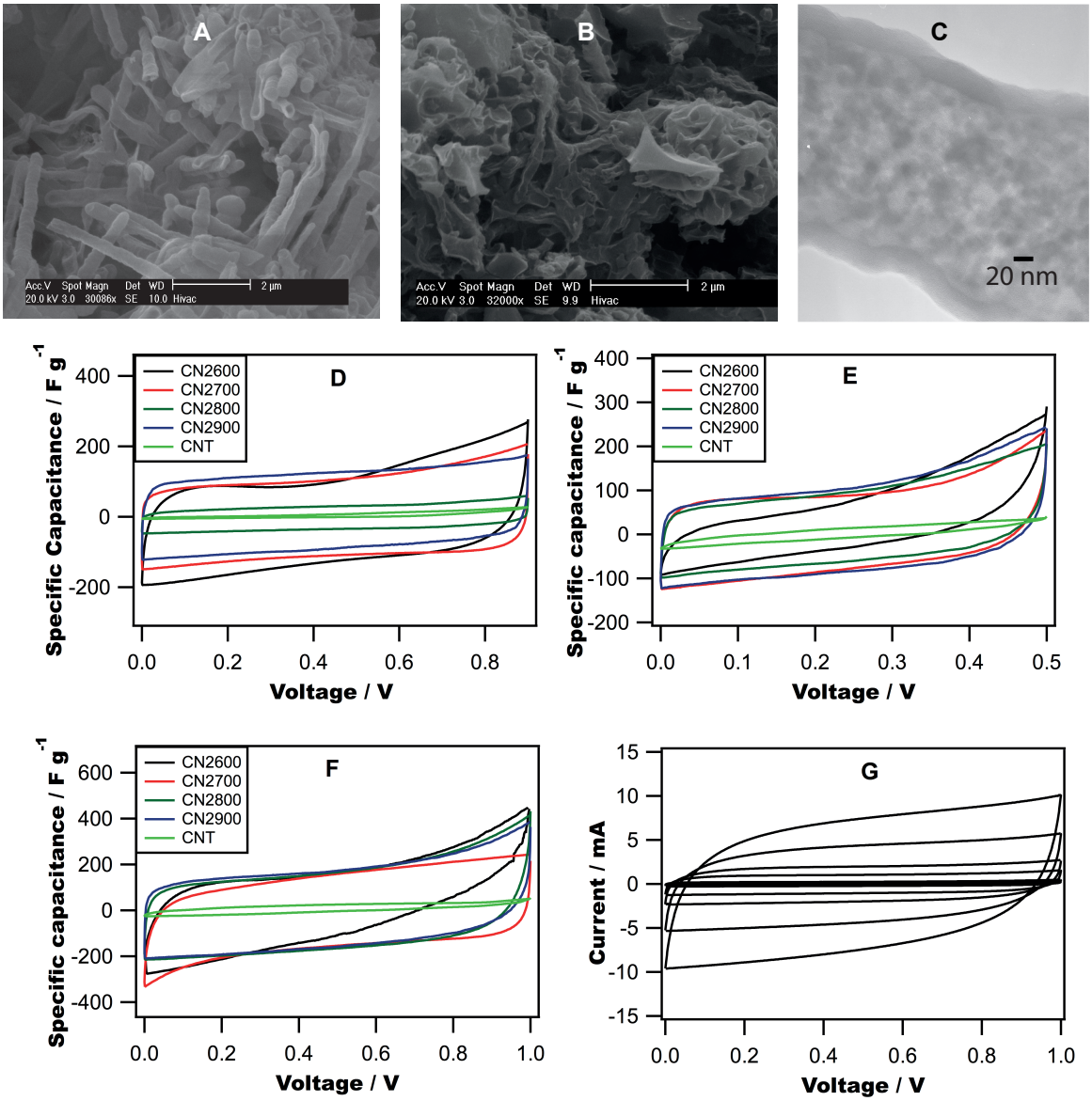

Figure 1. *(A) SEM image of acid-washed CNTs, (B) SEM image of material formed by activating CNTs at a C:KOH ratio of 2 and at 800 °C, (C) TEM image of material formed by activating CNTs at a C:KOH ratio of 2 and 600 °C. Parts D-F show CVs recorded at 5 mV* s^{-1} *in symmetrical EDLCs containing various carbons in (D) 2.0 M KCl, (E) 6.0 M KOH, and (F) 2.0 M* H_2SO_4*. Part G shows CVs recorded using EDLCs containing CN2900 electrodes and 2.0 M* H_2SO_4 *at (from bottom to top) 5 mV* s^{-1}*, 10 mV* s^{-1}*, 50 mV* s^{-1}*, 100 mV* s^{-1}*, 250 mV* s^{-1}*, and 500 mV* s^{-1}*. The scale bars in Parts A and B are 2 μm wide.*

inorganic material. XRD patterns of the CNTs and activated carbons (Figure S7 in the Supporting Information) all show a peak at $2\theta = 23°$, suggesting that the activated materials retain a similar level of graphitization as the as-synthesised material.

Figs. 1D-F show cyclic voltammograms (CVs) recorded using symmetrical EDLCs containing electrodes made with the various carbons, and aqueous KCl, KOH, and H_2SO_4, respectively, as electrolytes. In this figure, currents have been converted to C_s values using the relationship $C_s = 4I/mv$, where m is the total mass of carbon on the electrodes and v is the voltammetric scan rate.[48] While the CVs generally show the rectangular shape expected of capacitors, those recorded using carbons activated at higher temperatures (CN2700, CN2800 and CN2900) are more rectangular than those recorded using CN2600. In addition, those CVs recorded in acidic and neutral electrolyte are more rectangular than recorded using the alkaline electrolyte, most likely due to the high viscosity of the alkaline solution. Average C_s values are shown in Table 1, which shows that C_s is generally higher in the acidic electrolyte. It is also clear from the data in Table 1 that increasing the activation temperature results in an increase in C_s and the CN2900 sample has a C_s of 172 F g^{-1} in H_2SO_4, which is drastically higher than expected for a CNT-based electrode material,[40] as high as that expected for ACs in aqueous electrolytes,[4] and higher than recorded for graphene in aqueous and organic media.[49] Figure 3G shows the effect of v on the CVs recorded using CN2900 sample in H_2SO_4, and demonstrates that the rectangular shape is retained in the aqueous electrolyte up to at least 0.5 V s^{-1}, indicating that ion transport throughout the carbon structure was fast.

Given that the combination of the CN2900 sample and H_2SO_4 electrolyte seemed most promising for EDLCs, this combination was further analysed using galvanostatic charge-discharge (GCD) analysis (Figure 2A). In each case, an approximately symmetrical charge-discharge curve was obtained, as expected for a predominantly capacitive response when

Table 1. *Specific capacitance of CNT samples activated at 600, 700, 800 and 900 °C containing H_2SO_4, KCl, KOH, [EMIM][BF_4], and [BMIM][BF_4], respectively, as electrolytes determined using cyclic voltammetry (CV) and analysis of galvanostatic charge-discharge curves (GCD).*

		C_s (F g^{-1})			
Electrolyte	Method	CN2600	CN2700	CN2800	CN2900
2.0 M H_2SO_4	CV	103	156	165	172
	GCD	71	125	125	133
2.0 M KCl	CV	97	102	120	128
	GCD	41	91	100	97
6.0 M KOH	CV	90	96	102	103
	GCD	12	45	67	70
[EMIM][BF_4]	CV	-	-	-	144
[BMIM][BF_4]	CV	-	-	-	150

charge propagation through the electrode structure is relatively fast. C_s values were obtained from the slopes of the discharge curves recorded using each sample (at 50% discharge) using $C_s = 4I/[m(\mathrm{d}V/\mathrm{d}t)]$ (where m is the total mass of carbon on the electrodes and $\mathrm{d}V/\mathrm{d}t$ is the slope of the discharge curve)[48] and are also shown in Table 1. In general, the C_s values are slightly lower than those determined from the CV analysis (most likely due to the error associated with extracted C_s values from the slightly non-linear GCD curves) but the general trend is the same, with the CN2900/H_2SO_4 combination yielding the highest C_s. Fig. 2B shows a decrease in C_s of about 25% upon increasing the discharge current density from 0.1 A g^{-1} to 10 A g^{-1}. However, most of the C_s drop occurs below 2 A g^{-1} and the large current density range in which C_s remained near 100 F g^{-1} is promising for the development of devices that require operation over a range of current densities.

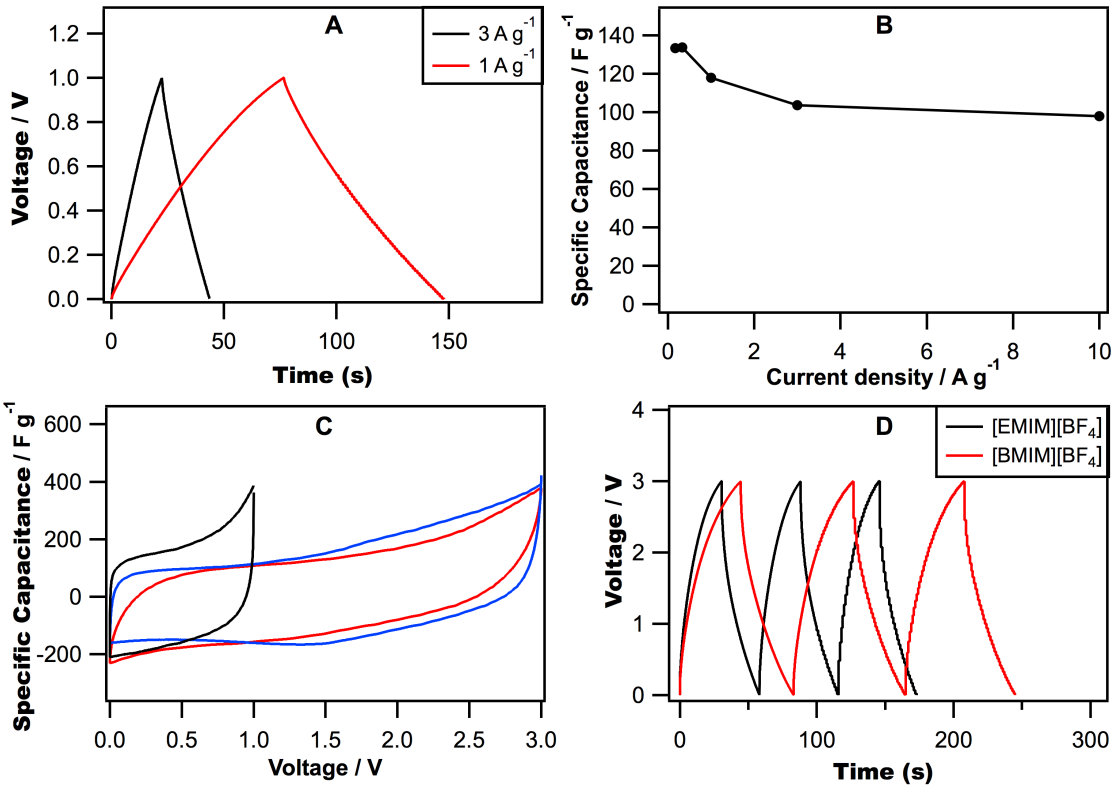

Figure 2. *(A) Galvanostatic charge-discharge curves recorded using symmetrical EDLCs containing CN2900 electrodes and 2.0 M H_2SO_4 at 1 A g^{-1} and 3 A g^{-1}. (B) Effect of increasing the discharge current density on the specific capacitance of the CN2900 electrodes. (C) CVs recorded at 5 mV s^{-1} using cells containing CN2900 electrodes and (black line) aqueous H_2SO_4, (red line) [EMIM][BF_4] and (blue line) [BMIM][BF_4]. (D). Galvanostatic charge/discharge currents recorded using cells containing CN2900 electrodes and (black line) [EMIM][BF_4] and (red line) [BMIM][BF_4].*

The high C_s of the activated samples can be rationalised by examining their porosity and, in particular, pore-size distributions (PSDs). Samples CN2600 and CN2700 exhibit Type-1 isotherms typical of microporous materials, while the isotherms of CN2800, and particularly CN2900, show evidence of the presence of both micropores and significant mesoporosity (Figure 3A). Therefore, there is a shift from microporosity to mesoporosity as the activation

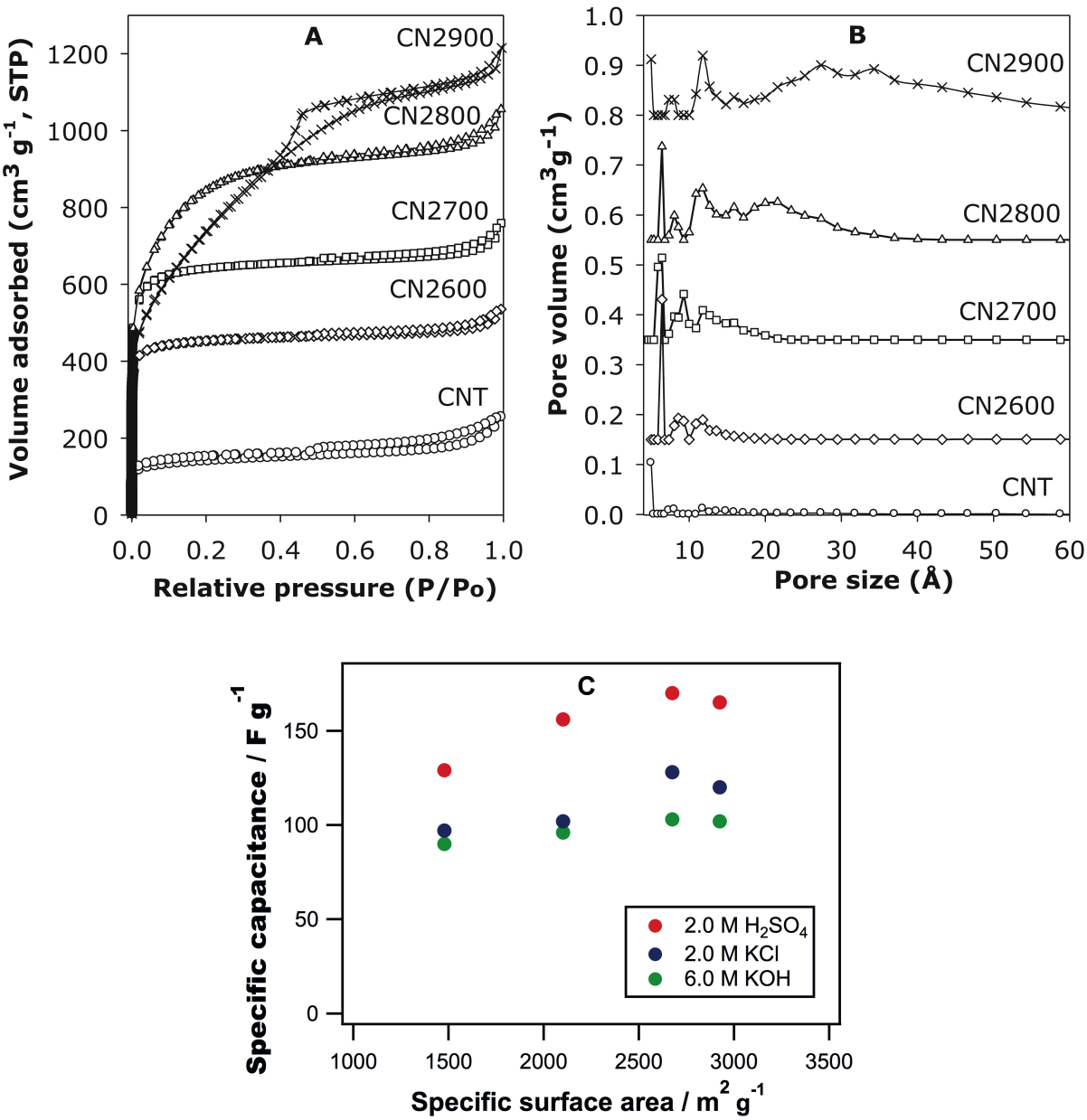

Figure 3. *(A) Nitrogen sorption isotherms and (B) pore size distribution curves of carbon samples. (C) Plot of specific capacitance versus the specific surface area of the activated samples in 2.0 M H_2SO_4, 2.0 M KCl and 6.0 M KOH.*

temperature increases. The PSD curves (Figure 3B) show that the CN2600 sample is made up mostly of narrow micropores with sizes below 7 Å (Table S1 in the Supporting Information). However, as the activating temperature increases, the proportion of larger pores

between 8 and 13 Å increases, to the extent that sample CN2900 shows a new pore maximum at 13 Å, along with a large proportion of mesopores in the range 20-50 Å. Furthermore, upon activation at successively higher temperatures, the SSAs increase from 1479 $m^2 g^{-1}$ for CN2600 to 2676 $m^2 g^{-1}$ for CN2900, with micropore surface areas of 1400 $m^2 g^{-1}$ and 801 $m^2 g^{-1}$, respectively. Therefore, the high proportion of mesopores in the CN2900 sample allows access of charge-balancing counterions to the carbon surface during charging/discharging. It is also notable that the sample activated at 800 °C has the highest BET SSA (2925 $m^2 g^{-1}$, which approaches that of activated graphene[33]) but with a larger proportion (ca. 87%) of the surface area arising from micropores, demonstrating that inaccessibility of the carbon surface to counterions limits C_s at very high SSAs (Fig. 3C).[50] These results demonstrate that the high C_s of the CN2900 sample results from a trade-off between the high mesoporosity, which allows access of ions during charging/discharging, and the high SSA imparted by activation.

One of the most promising strategies for increasing V is to use ionic liquids as they can exhibit potential windows up to 5-V wide and so can potentially be used to fabricate high-E_s devices.[51-53] Figure 2C shows the CVs obtained when the EDLCs contain [EMIM][BF_4] and [BMIM][BF_4] as electrolytes and the CN2900 sample as the electrode material. As shown by the red and blue lines, approximately rectangular responses are obtained over a much wider potential range than when using the aqueous H_2SO_4 electrolyte (black line in Figure 2C). Figure 2D shows that approximately symmetrical charge-discharge curves are recorded over a 3-V range. C_s values were determined using the CVs recorded at 5 mV s^{-1} and are 144 F g^{-1} and 150 F g^{-1} for the cells containing [EMIM][BF_4] and [BMIM][BF_4], respectively. These values are significantly higher than typically recorded using ionic liquids and high-SSA carbons as the relatively large ions usually cannot access porous carbon surfaces (C_s of high-SSA carbons is typically of the order of 100 F g^{-1} in the presence of ionic liquids).[7,54] In fact, these values are typical of that expected for porous carbons in aqueous

electrolytes,[24] a phenomenon that may be attributed to uniquely accessible, mesoporous electrode structure.

Electrochemical impedance spectroscopy (EIS) was carried out on each EDLC to further explore the effects of changing the electrode materials and electrolytes on mass and charge transport in the electrodes. Nyquists plots obtained from EIS of the EDLCs containing the aqueous and ionic liquid electrolytes and are shown in Figure 4. In the Nyquist plots, the lower left portions of the curves correspond to the higher frequencies and the right portion to lower frequencies. Upon changing the electrode material from CN2600 to CN2700, CN2800, and CN2900, the plots recorded using the aqueous cell become successively more vertical in the low-frequency regions (Figure 4A), indicating that the behaviour becomes more dominated by capacitance upon changing to the carbon activated at higher temperatures. Only the CN2600 sample exhibits a Warburg-like (approximately 45° line) response as the frequency changes, due to the impedance associated with diffusion of ions into the more microporous material. The responses from the cells containing the ionic liquids show a high-frequency semi-circle, a Warburg-type (45°) response upon entering the low-frequency region and similar gradients to each other in the low frequency region. The high-frequency intercepts in each plot are associated with the solution resistance and, as expected, the resistances are similar for the cells containing H_2SO_4. The high-frequency intercepts are higher when using the ionic liquids than when using the aqueous electrolytes, due to the higher resistance of the ionic media, and the intercept is slightly higher for the [BMIM]-containing cell than the [EMIM]-containing cell due to the lower conductivity of the liquid containing the larger cation.[55] The semicircles in Figure 4B are associated with charge-transfer resistance, and their absence from the plots obtained using the cell containing H_2SO_4 indicates that charge transfer is significantly faster in the cells containing the aqueous electrolytes.

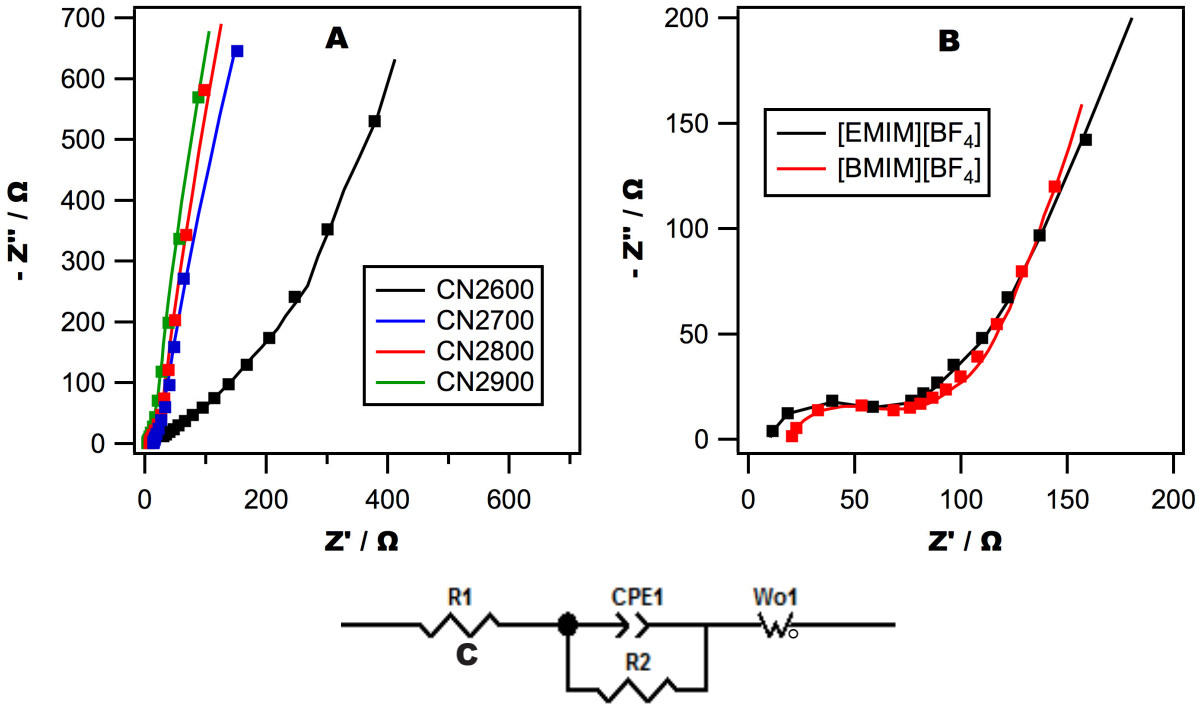

Figure 4. *Nyquist plots recorded in the frequency range 100 kHz-0.01 Hz using symmetrical EDLC cells containing (A) 2.0 M H_2SO_4 and (B) [EMIM][BF_4] and [BMIM][BF_4] (solid lines). The Nyquist plots were fitted to the Randles equivalent circuit shown in C with best-fit values shown in Table S2 in the Supporting Information. Fits to the data are shown by the markers.*

Each experimental Nyquist plot could be fitted to the simple equivalent circuit shown in Figure 4C and in which R_1 represents the solution resistance, R_2 is the charge-transfer resistance, Wo1 is a Warburg impedance, and CPE is a constant phase element, introduced to account for non-ideality of the rough electrode surfaces. The impedance of the CPE is given by $z_{\mathrm{CPE}} = Yi\omega^{-n}$, where ω is the angular frequency, i is $\sqrt{-1}$, and Y and n are fitting parameters (where n = 1 for a pure capacitor). Wo1 represents the impedance due to ion diffusion from the electrolyte and comprises the ohmic resistance (*W*–*R*), the diffusion time constant (*W*–*T*), and Warburg exponent (*W*–*P*). The best-fit values of all circuit parameters

are shown in the Tables S2 and S3 in the Supporting Information and show that n was almost 1 in each case. From the best-fit parameters in Tables S2 and S3, it is clear that the capacitance terms generally increase upon successively changing the electrode material from CN2600 to CN2900 in the aqueous electrolytes and that the resistance terms decreased accordingly. The higher resistance of [BMIM][BF_4] than [EMIM][BF_4] is also evident from the fitting data, as is the higher diffusion resistance of the ionic liquid electrolytes.

The electrochemical stability of the CN2900 was examined using potential cycling in the aqueous and ionic liquid electrolytes at 0.1 A g^{-1} and Figures S8-S11 in the Supporting Information shows that the capacitance retention was above 90% over the first 1000 charge/discharge cycles and 80% over 4000 cycles for the H_2SO_4-containing cell. In the case of the ionic liquid ([EMIM][BF_4])-containing cell, the capacitance retention was above 90% over 4000 charge-discharge cycles when the cell was charged to 2 V, and 80% when the cell was charged to 3 V. The lower stability of the ionic liquid-when charged to the higher voltage is most likely due to irreversible reactions between the ionic liquid and the carbon surface at higher voltages, a factor that may be resolved by fine-tuning of the ionic liquid composition.[53]

The specific energy and power, E_s and P_s, respectively, of the EDLCs containing the ionic liquid electrolytes were determined using the relationships $E_s = \frac{1}{8} C_s V^2$, where V is the voltage window of the EDLC, and $P_s = E_s/\Delta t_d$, where Δt_d is the discharge time. E_s is 45 Wh kg^{-1} and 47 Wh kg^{-1} in [EMIM][BF_4] and [BMIM][BF_4] at P_s = 4.0 kW kg^{-1} and 4.3 kW kg^{-1}, respectively (based on the mass of carbon within the devices). Therefore, the combination of CN2900 and the ionic liquid ranks these materials among the highest-energy materials for supercapacitor devices (including those containing high-SSA carbons, and pseudocapacitive heteroatom-doped carbons, metal oxides, and conducting polymers).[10,11,15,16,23,33,56-64] In the presence of aqueous H_2SO_4, E_s = 5.9 Wh kg^{-1} at a power of 1.0 kW kg^{-1}. As has been pointed

out recently, it is also useful to compare specific energies and powers in context of full, packaged EDLCs, given that the packaging material, electrolytes *etc*. can comprise a significant mass of the full device.[48] Assuming that 30% of the mass of a packaged EDLC comprises the electrode material, which is typical for an AC-based device,[33] then practical energy densities of about 15 Wh kg^{-1} can be estimated for the ionic liquid-based systems which is three times larger than that of a typical packaged AC-based EDLC, higher than that of many new "high-end" EDLC devices[16] and devices based on pseudocapacitive conducting polymers,[23] and about as large as the energy density of a lead-acid battery.[33] In addition, the power (up to ~10 kW kg^{-1}) at which high energies can be delivered exceeds that achievable by most battery systems. These performance characteristics are best illustrated by the Ragone plot in Figure 5, which shows the energy and power densities of various electrochemical energy storage devices, when compared to our devices when charged and discharged at a range of powers (red and blue crosses). Clearly, the use of the CNT-based electrodes with the aqueous electrolyte results in a device that competes with the best EDLC systems available in terms of the mass-specific energy density, but which can achieve higher power at lower energies due to the mesoporosity of the carbon electrode materials. The use of the ionic liquid electrolyte, on the other hand, pushes the performance towards much higher energy densities and the devices clearly bridge the performance gap between conventional EDLCs and higher-energy Ni-MH, Li-ion and lead-acid battery systems. In other words, the combination of the CN2900 carbon as electrode material and ionic liquid electrolyte results in a device with energy density comparable to those of Ni-MH and lead-acid batteries but which can be charged and discharged in minutes.

It is important to note that the mass-specific energy and power are not the only factors that must be considered when developing a new electrode material for EDLCs. As has been pointed out by Gogotsi and Simon, many nanomaterials have low packing densities and, when

incorporated into actual devices, the void areas will be flooded by electrolyte, potentially increasing the mass of the device significantly but without increasing its capacitance.[63] Therefore, the volumetric energy density of the devices should also be considered, particularly if thin-film devices, in which the mass of electrode materials is quite small, are to be fabricated. The density, ρ, of our CN2900 electrode material was determined using the following equation:

$$\rho \text{ (g cm}^{-3}) = \left(V_{\text{tot}} + \frac{1}{\rho_{\text{T}}} \right)^{-1} \quad (1)$$

where V_{tot} is the total pore volume (1.88 cm^3 for CN2900) and ρ_{T} is the true density of carbon (2.2 g cm^{-3}). Using Equation 1, ρ = 0.43 g cm^{-3}, so the volumetric energy density of the material in the presence of, for example, [BMIM][BF_4] is 20.2 Wh L^{-1} for the material and ~6 Wh L^{-1} for the device, which is very similar to that achievable by commercially-available cells. Therefore, thin film devices with performances comparable to those of commercially-available devices could also be fabricated using our carbons. However, as described above, devices with dimensions comparable to those of commercial systems (100 to 200-μm thick films or about 10 mg/cm^2 of carbon film), in which the mass specific energy density is important,[63] will benefit particularly from the use of the materials described here and will offer energy storage/delivery solutions when simultaneous high energy and high power is required.

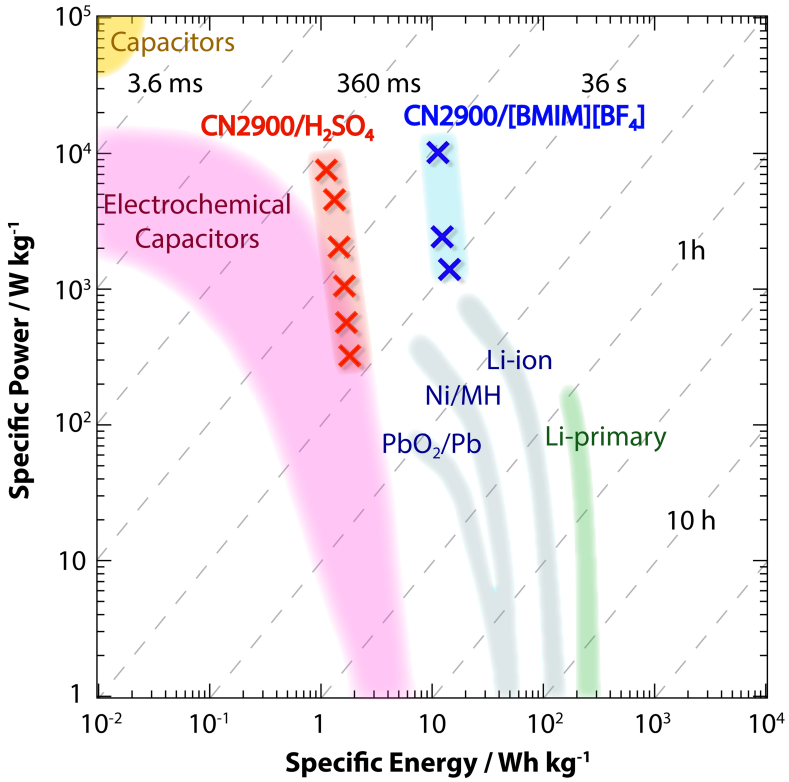

Figure 5. *Ragone plot of specific power versus specific energy for various electrochemical energy storage devices. The times shown are the time constants of the devices, which are obtained by dividing the energy by the power. Also shown are the specific energy and specific power of the aqueous (red crosses) and ionic liquid-based (blue crosses) symmetric EDLCs containing CN2900 electrodes. Ni/MH is the nickel metal hydride battery system.*

4. Conclusions

By chemically activating CNTs that are synthesised at 180 °C, porous carbons with specific BET surface areas higher than that of pristine graphene can be made and are extremely promising electrode materials for high-energy/high-power EDLCs. The best performing material, which is that activated at 900 °C and at a CNT/KOH ratio of 2, is highly mesoporous and yields specific capacitances of 172 F g^{-1} in acidic media and 150 F g^{-1} in the ionic liquid [BMIM][BF_4], remarkable values that are attributed to the accessibility of the

mesoporous carbon surface to counterions during charging/discharging of the material. The estimated volume-specific energy density of devices containing ionic liquid electrolytes competes with that achievable using commercially-available devices containing AC electrodes. However, when the mass specific energy and power of the ionic liquid system are considered, which is particularly important for devices with dimensions similar to those of commercial devices, the device performance bridges the gap between that of conventional EDLCs and common battery systems. The particular combination of the CN2900 carbon electrode material with [BMIM][BF_4] as the electrolyte results in a device with an energy density comparable to those of Ni-MH and lead-acid batteries but which, due to its ability to work at high powers, can be recharged in minutes. In addition to the excellent performance characteristics of the electrode materials, it is remarkable that the methods used to produce our electrode materials are very simple, scalable, and can be carried out in most laboratories with common laboratory equipment. Such readily-available materials could quite easily replace the state-of-the-art materials in commercial devices when simultaneous high energy and high power is a priority.

Acknowledgements

We thank the University of Nottingham for funding HMC's PhD studentship.

References

1. N.-S. Choi, Z. Chen, S. A. Freunberger, X. Ji, Y.-K. Sun, K. Amine, G. Yushin, L. F. Nazar, J. Cho, P. G. Bruce, *Angew. Chem. Int. Ed.*, 2012, **51**, 9994-10024.
2. B. Dunn, H. Kamath, J. M. Tarascon, *Science*, 2011, **334**, 928-935.
3. J. R. Miller, P. Simon, *Science*, 2008, **321**, 651-652.
4. P. Simon, Y. Gogotsi, *Nat. Mater.*, 2008, **7**, 845-854.

5. P. J. Hall, M. Mirzaeian, S. I. Fletcher, F. B. Sillars, A. J. R. Rennie, G. O. Shitta-Bey, G. Wilson, A. Cruden, R. Carter, *Energy Environ. Sci.*, 2010, **3**, 1238-1251.

6. P. Simon, Y. Gogotsi, *Acc. Chem. Res*, 2013, **46**, 1094-1103.

7. W.-Y. Tsai, R. Lin, S. Murali, L. Li Zhang, J. K. McDonough, R. S. Ruoff, P.-L. Taberna, Y. Gogotsi, P. Simon, *Nano Energy*, 2013, **2**, 403-411.

8. M. V. Fedorov, A. A. Kornyshev, *Chem. Rev.*, 2014, **114**, 2978-3036.

9. G. Milczarek, A. Ciszewski, I. Stepniak, *J. Power Sources*, 2011, **196**, 7882-7885.

10. C. Zhang, D. Long, B. Xing, W. Qiao, R. Zhang, L. Zhan, X. Liang, L. Ling, *Electrochem. Commun.*, 2008, **10**, 1809-1811.

11. L.-F. Chen, X.-D. Zhang, H.-W. Liang, M. Kong, Q.-F. Guan, P. Chen, Z.-Y. Wu, S.-H. Yu, *ACS Nano*, 2012, **6**, 7092-7102.

12. H. M. Jeong, J. W. Lee, W. H. Shin, Y. J. Choi, H. J. Shin, J. K. Kang, J. W. Choi, *Nano Lett.*, 2011, **11**, 2472-2477.

13. X. Yu, H. S. Park, *Carbon*, 2014, **77**, 59-65.

14. D. Zhang, L. Zheng, Y. Ma, L. Lei, Q. Li, Y. Li, H. Luo, H. Feng, Y. Hao, *ACS. Appl. Mater. Interfaces*, 2014, **6**, 2657-2665.

15. Z. Tang, C.-h. Tang, H. Gong, *Adv. Funct. Mater.*, 2012, **22**, 1272-1278.

16. J. Ji, L. L. Zhang, H. Ji, Y. Li, X. Zhao, X. Bai, X. Fan, F. Zhang, R. S. Ruoff, *ACS Nano*, 2013, **7**, 6237-6243.

17. S. W. Lee, J. Kim, S. Chen, P. T. Hammond, Y. Shao-Horn, *ACS Nano*, 2010, **4**, 3889-3896.

18. Z. Fan, J. Yan, T. Wei, L. Zhi, G. Ning, T. Li, F. Wei, *Adv. Funct. Mater.*, 2011, **21**, 2366-2375.

19. Q. Cheng, J. Tang, N. Shinya, L.-C. Qin, *J. Power Sources*, 2013, **241**, 423-428.

20. K. Zhang, L. L. Zhang, X. S. Zhao, J. Wu, *Chem. Mater.*, 2010, **22**, 1392-1401.

21. J. Li, H. Xie, Y. Li, *J. Power Sources*, 2013, **241**, 388-395.

22. L. Lai, L. Wang, H. Yang, N. G. Sahoo, Q. X. Tam, J. Liu, C. K. Poh, S. H. Lim, Z. Shen, J. Lin, *Nano Energy*, 2012, **1**, 723-731.

23. G. A. Snook, P. Kao, A. S. Best, *J. Power Sources*, 2011, **196**, 1-12.

24. L. L. Zhang, X. S. Zhao, *Chem. Soc. Rev.*, 2009, **38**, 2520-2531.

25. A. G. Pandolfo, A. F. Hollenkamp, *J. Power Sources*, 2006, **157**, 11-27.

26. D. Lozano-Castelló, D. Cazorla-Amorós, A. Linares-Solano, S. Shiraishi, H. Kurihara, A. Oya, *Carbon*, 2003, **41**, 1765-1775.

27. J. H. Chae, G. Z. Chen, *Electrochim. Acta*, 2012, **86**, 248-254.

28. J. Chmiola, G. Yushin, Y. Gogotsi, C. Portet, P. Simon, P. L. Taberna, *Science*, 2006, **313**, 1760-1763.

29. Y. Zhai, Y. Dou, D. Zhao, P. F. Fulvio, R. T. Mayes, S. Dai, *Adv. Mater*, 2011, **23**, 4828-4850.

30. E. Frackowiak, *Phys. Chem. Chem. Phys.*, 2007, **9**, 1774-1785.

31. E. Frackowiak, F. Beguin, *Carbon*, 2001, **39**, 937-950.

32. J. Yan, J. Liu, Z. Fan, T. Wei, L. Zhang, *Carbon*, 2012, **50**, 2179-2188.

33. Y. Zhu, S. Murali, M. D. Stoller, K. J. Ganesh, W. Cai, P. J. Ferreira, A. Pirkle, R. M. Wallace, K. A. Cychosz, M. Thommes, D. Su, E. A. Stach, R. S. Ruoff, *Science*, 2011, **332**, 1537-1541.

34. M. Kaempgen, C. K. Chan, J. Ma, Y. Cui, G. Gruner, *Nano Lett.*, 2009, **9**, 1872-1876.

35. K. H. An, W. S. Kim, Y. S. Park, Y. C. Choi, S. M. Lee, D. C. Chung, D. J. Bae, S. C. Lim, Y. H. Lee, *Adv. Mater*, 2001, **13**, 497-500.

36. R. Ma, J. Liang, B. Wei, B. Zhang, C. Xu, D. Wu, *Bull. Chem. Soc. Jpn.*, 1999, **72**, 2563-2566.

37. Y. Honda, T. Haramoto, M. Takeshige, H. Shiozaki, T. Kitamura, M. Ishikawa, *Electrochem. Solid-State Lett.*, 2007, **10**, A106-A110.

38. S. M. Lee, S. C. Lee, J. H. Jung, H. J. Kim, *Chem. Phys. Lett.*, 2005, **416**, 251-255.

39. B. Xu, F. Wu, Y. Su, G. Cao, S. Chen, Z. Zhou, Y. Yang, *Electrochim. Acta*, 2008, **53**, 7730-7735.

40. Q. Jiang, M. Z. Qu, G. M. Zhou, B. L. Zhang, Z. L. Yu, *Mater. Lett.*, 2002, **57**, 988-991.

41. Y. Liu, Z. Shen, K. Yokogawa, *Mater. Res. Bull.*, 2006, **41**, 1503-1512.

42. P.-L. Taberna, G. Chevallier, P. Simon, D. Plée, T. Aubert, *Mater. Res. Bull.*, 2006, **41**, 478-484.

43. F. Zhang, J. Tang, N. Shinya, L.-C. Qin, *Chem. Phys. Lett.*, 2013, **584**, 124-129.

44. B. Adeniran, R. Mokaya, *J. Mater. Chem. A*, 2015, **3**, 5148-5161.

45. M. Kumar, Y. Ando, *J. Nanosci. Nanotechnol.*, 2010, **10**, 3739-3758.

46. P. Bonhôte, A. P. Dias, N. Papageorgiou, K. Kalyanasundaram, M. Grätzel, *Inorg. Chem.*, 1996, **35**, 1168-1178.

47. J. D. Holbrey, W. M. Reichert, R. P. Swatloski, G. A. Broker, W. R. Pitner, K. R. Seddon, R. D. Rogers, *Green Chem.*, 2002, **4**, 407-413.

48. M. D. Stoller, R. S. Ruoff, *Energy Environ. Sci.*, 2010, **3**, 1294-1301.

49. M. D. Stoller, S. Park, Y. Zhu, J. An, R. S. Ruoff, *Nano Lett.*, 2008, **8**, 3498-3502.

50. P. Simon, A. Burke, *Interface*, 2008, **17**, 38-43.

51. D. R. MacFarlane, N. Tachikawa, M. Forsyth, J. M. Pringle, P. C. Howlett, G. D. Elliott, J. H. Davis, M. Watanabe, P. Simon, C. A. Angell, *Energy Environ. Sci.*, 2014, **7**, 232-250.

52. A. Lewandowski, A. Olejniczak, M. Galinski, I. Stepniak, *J. Power Sources*, 2010, **195**, 5814-5819.

53. K. L. Van Aken, M. Beidaghi, Y. Gogotsi, *Angew. Chem. Int. Ed.*, 2015, **54**, 4806-4809.

54. A. Balducci, R. Dugas, P. L. Taberna, P. Simon, D. Plee, M. Mastragostino, S. Passerini, *J. Power Sources*, 2007, **165**, 922-927.

55. A. Stoppa, O. Zech, W. Kunz, R. Buchner, *J. Chem. Eng. Data*, 2010, **55**, 1768-1773.

56. H. Wang, Z. Xu, A. Kohandehghan, Z. Li, K. Cui, X. Tan, T. J. Stephenson, C. K. King'ondu, C. M. B. Holt, B. C. Olsen, J. K. Tak, D. Harfield, A. O. Anyia, D. Mitlin, *ACS Nano*, 2013, **7**, 5131-5141.

57. D.-W. Wang, F. Li, M. Liu, G. Q. Lu, H.-M. Cheng, *Angew. Chem. Int. Ed.*, 2007, **47**, 373-376.

58. Y. Wang, Z. Shi, Y. Huang, Y. Ma, C. Wang, M. Chen, Y. Chen, *J. Phys. Chem. C*, 2009, **113**, 13103-13107.

59. B. G. Choi, M. Yang, W. H. Hong, J. W. Choi, Y. S. Huh, *ACS Nano*, 2012, **6**, 4020-4028.

60. V. V. N. Obreja, *Physica E*, 2008, **40**, 2596-2605.

61. A. Izadi-Najafabadi, S. Yasuda, K. Kobashi, T. Yamada, D. N. Futaba, H. Hatori, M. Yumura, S. Iijima, K. Hata, *Adv. Mater*, 2010, **22**, E235-E241.

62. S. Bose, T. Kuila, A. K. Mishra, R. Rajasekar, N. H. Kim, J. H. Lee, *J. Mater. Chem.*, 2012, **22**, 767-784.

63. Y. Gogotsi, P. Simon, *Science*, 2011, **334**, 917-918.

64. Q. Cheng, J. Tang, J. Ma, H. Zhang, N. Shinya, L.-C. Qin, *Phys. Chem. Chem. Phys.*, 2011, **13**, 17615-17624.